Characterization of high-speed balanced photodetectors

Article (Accepted Version)

Characterization of high-speed balanced photodetectors

Paul Struszewski, Mark Bieler, David Humphreys, *Senior Member, IEEE*, Hualong Bao, Marco Peccianti, and Alessia Pasquazi

***Abstract*—We report the characterization of a balanced ultrafast photodetector. For this purpose we use a recently developed time-domain laser-based vector network analyzer to determine the common mode rejection ratio of device under test. This includes the frequency-domain response above the single-mode frequency of the coaxial connector. Although the balanced photodetector has a nominal bandwidth of 43 GHz, it generates voltage pulses with frequency components up to 180 GHz. We obtain a common mode rejection ratio of better than 30 dB up to 70 GHz and better than 20 dB up to 110 GHz. The laser-based measurements are compared to measurements using a digital sampling oscilloscope and to frequency-domain measurements using a conventional VNA. We obtain good agreement between the three techniques with the laser-based method providing the largest measurement bandwidth although it also constitutes the most complicated characterization setup.**

***Index Terms*—differential photodetector, common mode rejection ratio, electrooptic sampling.**

I. Introduction

PHOTODETECTORS provide the link between optical and electronic signals and are essential components for a variety of applications. While single photodetectors [1]–[4] are mainly used for sensing applications, balanced photodetectors [5]–[7] are key precursor to hybrid detectors for coherent communications. Such coherent devices with 64 Gbaud data rate are commercially available [8] and proof-of-principle operation of 1.92 Tbaud over 225 km using polarization-multiplexed optical time-division multiplexing with a 170 GHz optical channel data rate has been demonstrated [9].

The accurate characterization of ultrafast single and balanced photodetectors is challenging since its bandwidth often exceeds the bandwidth of the utilized measuring devices. Previously, the frequency-response of single photodetectors has been characterized using a combination of an electrical vector network analyzer (VNA) and laser-based electro-optical sampling techniques up to a frequency of 110 GHz [10]. Yet, this method will not be suitable to determine the impulse response of the photodetector if frequencies above 110 GHz contain significant power. Recently, this problem could be circumvented employing laser-based techniques only, such that the time-domain response of a single photodetector was obtained [11].

In this paper we address the common-mode rejection-ratio (CMRR) characterization of a balanced high-speed photodetector [5]–[7]. The test device has a nominal bandwidth of 43 GHz and is representative of the devices used in current systems. We also determine the CMRR of the test device using a Digital Sampling Oscilloscope (DSO) and a Vector Network Analyzer (VNA) with the aim of finding the limitation of such approaches.

The preliminary findings of this work have been published in the CPEM 2016 conference proceedings [11]. The present work extends [11] by two main aspects: First, we outline the algorithms to determine the optimized CMRR, from imperfect measured results. For example, the optical delay, optical coupling or device leakage current may be different for each diode of the pair, adversely affecting the CMRR measurement. Second, we compare the laser-based measurements with DSO and conventional VNA measurements. The good agreement between the different methods validates our results.

This paper is organized as follows: In Sec. II we introduce the CMRR and the optimization procedure, the Electro-Optic Sampling (EOS) measurements are discussed in Sec. III, and Sec. IV describes the measurements made with commercial instrumentation. In Sec. V the results from each system are compared, the key findings are summarized, and conclusions are made.

II. Common Mode Rejection Ratio

At first a remark on the notation is necessary. Throughout this paper lower- and upper-case variables denote time- and frequency domain signals, respectively, with the time and frequency dependence being taken as implicit.

The standard definition for CMRR used for electrical components, such as operational amplifiers is

$$CMRR = 20 \cdot \log\left(\left|\frac{V_\mathrm{p} - V_\mathrm{n}}{V_\mathrm{p} + V_\mathrm{n}}\right|\right), \tag{1}$$

Submission date: 2016-07-11. This work was supported in part by the European Metrology Research Programme (EMRP) through the Joint Research Projects IND16 entitled Metrology for Ultrafast Electronics and High-Speed Communications and IND51 entitled Metrology for Optical and RF Communications Systems. The EMRP is jointly funded by the EMRP participating countries within EURAMET and the European Union. P.S. acknowledges support by the Braunschweig International Graduate School of Metrology B-IGSM and the DFG Research Training Group GrK1952/1 "Metrology for Complex Nanosystems". H.B, M.P., and AP acknowledge support from the UK Quantum Technology Hub for Sensors and Metrology, EPSRC grant EP/M013294/1.

Paul Struszewski and Mark Bieler are with the Physikalisch-Technische Bundesanstalt, Bundesallee 100, 38116 Braunschweig, Germany (email: pauls.struszewski@ptb.de; mark.bieler@ptb.de).

David Humphreys is with the National Physical Laboratory, Hampton Rd, Teddington, Middlesex TW11 0LW, U.K. (e-mail: david.humphreys@npl.co.uk).

Bao Hualong, Marco Peccianti, and Alessia Pasquazi are with the Emergent Photonics Laboratory (EPic), of the University of Sussex, Brighton BN1 9QH, U.K. (email: baohualong@gmail.com, m.peccianti@sussex.ac.uk, a.pasquazi@sussex.ac.uk).

where V_p and V_n are the positive and negative voltage inputs, respectively.

This definition is satisfactory for electronic systems but in a high-bandwidth differential photodiode, the two devices will have some design differences to provide the signal inversion. Also, the same average optical power applied to the input connectors may experience different delays and coupling losses from the optical fiber. Additionally, small differences in the light absorption profile mean that the dc current may not be a true reflection of the high-frequency response and therefore balancing the dc photocurrents or optical powers may not correspond to the maximum achievable CMRR.

To account for these imperfections we allow for small changes of the positive voltage by an amplitude factor α and a phase factor τ such that the optimized positive voltage is given by

$$V'_p(f,\alpha,\tau) = \alpha \exp(j\omega\tau) \cdot V_p(f), \tag{2}$$

with α and τ being chosen to minimize

$$E_{\min} = \min_{\alpha,\tau} \sum_f \left(\left| \frac{V'_p(f,\alpha,\tau) + V_n(f)}{V'_p(f,\alpha,\tau) - V_n(f)} \right| \right), \tag{3}$$

where the summation over f is done in a frequency range where V_p and V_n provide significant power.

After minimization of (3) we can express the optimized CMRR using the notation $V'_{p,opt} = V'_p(f, \alpha_{opt}, \tau_{opt})$ as

$$CMRR_{opt} = 20 \cdot \log \left(\left| \frac{V'_{p,opt} - V_n}{V'_{p,opt} + V_n} \right| \right). \tag{4}$$

At this position some remarks are meaningful. (4) is only valid if the measured difference signal $V_{diff,m}$ is identical to the calculated difference signal $V_{diff,c} = V_p + V_n$. If significant differences between the two signals exist, the device will be nonlinear. In this case the definition of the CMRR has to be revised by replacing $V_p + V_n$ in the nominator of (1) by $V_{diff,m}$. For the optimization we then have to minimize the following function

$$E_{\min} = \min_{\alpha,\tau} \sum_f \left(\left| \frac{V_{diff,m}(f) - V_p(f) + V'_p(f,\alpha,\tau)}{V'_p(f,\alpha,\tau) - V_n(f)} \right| \right). \tag{5}$$

Using again the symbol $V'_{p,opt}$ for the optimized positive voltage we then obtain for the optimized CMRR for the case of a nonlinear device

$$CMRR_{opt,NL} = 20 \cdot \log \left(\left| \frac{V'_{p,opt} - V_n}{V'_{p,opt} + V_n + V_{NL}} \right| \right), \tag{6}$$

which differs from (4) by having the additional term $V_{NL} = V_{diff,m} - V_{diff,c}$ in the nominator. We will show in Sec. III that the balanced detector under test is linear and (4) and (6) provide the same results.

It is important to note that if the CMRR is high (>20 dB) then V_p and $-V_n$ are approximately equal and so

$$V_p - V_n \approx 2V_p \approx -2V_n. \tag{7}$$

The error introduced into the result using this approximation and for a poor device is typically less than 0.5 dB.

III. Electro Optical Sampling

In this section we discuss CMRR measurements using a recently developed laser-based VNA. This device is described in detail in [12]; we only give a brief description here. We have evaporated a 4-mm long coplanar waveguide (CPW) onto a 500-μm thick substrate made of gallium arsenide (GaAs). The CPW is terminated on both sides with a microwave probe ending in a 1.85 mm coaxial connector. While the microwave probe on the left-hand side of the CPW is terminated with a 50 Ω load the microwave probe on the right-hand side is connected to the balanced photodetector, see Fig. 1. This setup is used to transfer the voltage pulses from the coaxial output of the photodetector to our coplanar measurement plane.

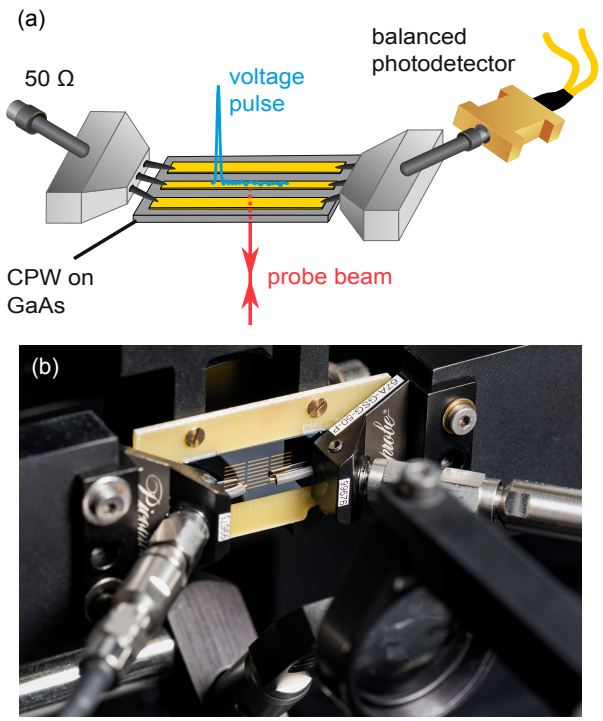

Fig. 1. (a) Main part of the experimental setup. Voltage pulses are detected after a propagation distance of approximately 2 mm on a 4 mm-long CPW. The probe beam is focused from the backside through the substrate onto the signal line of the CPW. (b) Picture of the main part of the experimental setup. Mirror images of the microwave probes occur on the GaAs wafer, on which several CPWs are visible.

The actual laser-based measurement of the voltage signals are carrier out as follows. A laser beam (100 fs pulse width, 1600 nm center wavelength), which is synchronized to the two laser beams exciting the differential photodetector, is focused from the backside of the GaAs substrate onto the signal line of the CPW. This laser beam is referred to as probe beam. When passing through the electric field of the voltage pulses the probe beam experiences a polarization change due to the electro-optic effect of the GaAs substrate. Guiding the back reflection of the probe beam to a typical electro-optic detection set-up we extract the polarization change, which is proportional to the electric field of the voltage pulses. By changing the time delay between the probe beam and the laser beams exciting the photodetector the shape of the voltage pulse is obtained. The time delay is changed with a motorized delay

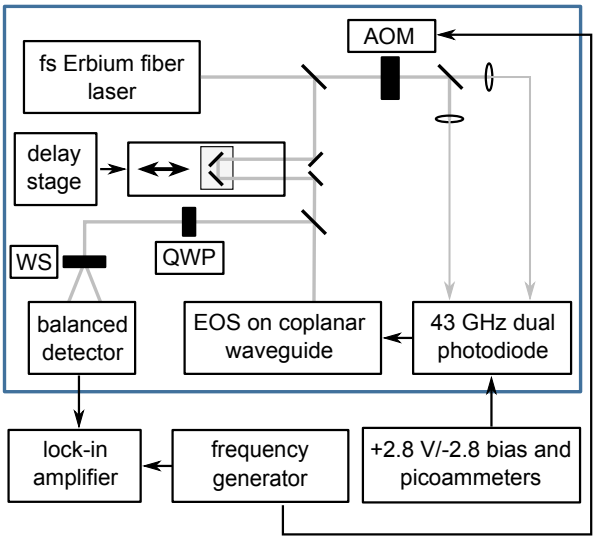

Fig. 2. System layout for the CMRR measurement using the electro-optical sampling (EOS) technique. AOM: acousto-optic modulator, QWP: quarter-wave plate, WP: Wollaston prism. The large blue rectangle surrounds the components placed on the optical bench.

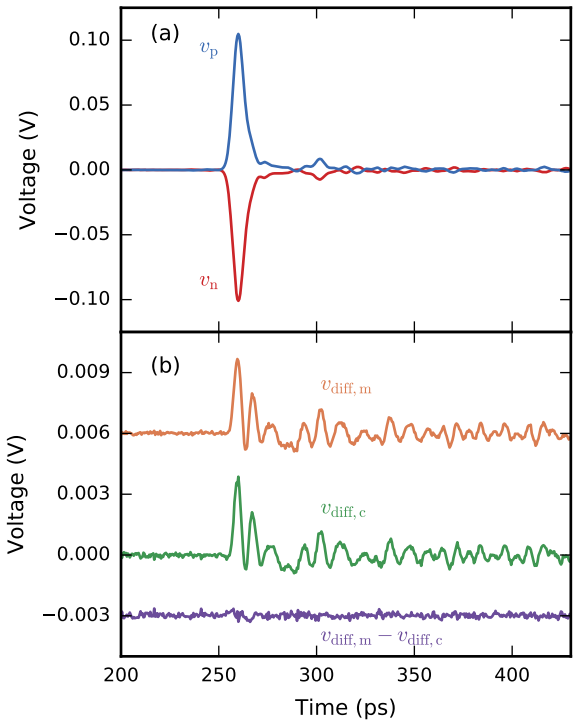

Fig. 3. (a) Voltage pulses generated from the balanced photodetector and sampled at the coplanar measurement plane using the femtosecond laser. The pulses v_p and v_n represent the voltage signals obtained by exciting the two photodiodes of the balanced device separately. (b) Green curve: calculated difference signal $v_{diff,c} = v_p - v_n$ of the individual measurements shown in (a). Orange curve: measured difference signal $V_{diff,m}$ when both diodes are illuminated simultaneously. Violet curve: difference between the measured and calculated difference signal. The orange and violet curves are shifted vertically for clarity.

line being calibrated to the unit of length [12]. This gives direct traceability of our measured time axis to the unit of time. A schematic layout of the whole experimental setup is shown in Fig. 2.

We like to note that measurement of two voltage pulses $v_1(t)$ and $v_2(t)$ at different positions on the CPW allows for the separation of forward and backward propagating voltage signals [12]. This in turn enables us to calculate the complex reflection coefficient at the CPW measurement plane and is, thus, identical to a one-port vector network analyzer, except that the measurements are carrier out in the time-domain. Yet, we do not have to determine reflection coefficients since any mismatch will cancel out during data analysis.

In Fig. 3(a) are shown the measured v_p and v_n obtained by exciting the two photodiodes of the balanced device separately. The measurements were carried out over a time epoch of 2 ns yielding a frequency spacing of 500 MHz. Yet, for better visualization we show the voltage pulses only over a limited temporal range of 225 ps. The measurements were carried out as follows. First we have adjusted the laser power for the two detector arms such that the same photocurrents are obtained. In a second step we have adjusted the delay between the excitation pulses of the two photodiodes of the balanced device. For this purpose several measurements of the voltage pulses were performed and the delay between the pulses was minimized to yield voltage pulse maxima at the same temporal instance.

This manual optimization yielded a difference signal, which is a factor of 30, i.e, approximately 30 dB smaller than the individual pulses, see Fig. 3(b) and corresponding frequency-domain behavior in Fig. 4. However, the individual signals v_p and v_n have slightly different amplitudes (ratio of 0.963) for the same photocurrents. This directly shows that the optimal CMRR is not obtained for equal photocurrents.

Before commenting on the optimization and calculation of the CMRR we discuss the linearity of the balanced detector. In Fig. 3(b) are shown the measured difference signal, the calculated difference signal $v_{diff,c} = v_p + v_n$, and the difference between the two signals corresponding to the term $v_{NL} = v_{diff,m} - v_{diff,c}$ introduced in Sec. II. It is clear that v_{NL} is almost identical to the noise, being approximately 44 dB below the voltage pulse amplitude of v_p and v_n.

Due to the fact that v_{NL} is vanishing within the noise we have first used (4) to optimize the CMRR. The result $CMRR_{opt}$ is shown in Fig. 5 up to a frequency of 225 GHz and we take this plot as the best estimate of the CMRR of the device under test obtained from the laser-based electro-optic sampling measurements. We obtain a common mode rejection ratio of better than 40 dB up to 20 GHz, better than 30 dB up to 70 GHz, and better than 20 dB up to 110 GHz. It should be noted that the spectra of V_p and V_n approach the noise limit at approximately 180 GHz. The light, semitransparent colors in Fig. 5 denote the 95% confidence intervals obtained from Monte-Carlo calculations. Theses uncertainty evaluations were performed in the same manner as described in [12].

The very sharp peaks of $CMRR_{opt}$ between 50 GHz and 80 GHz and between 110 GHz and 150 GHz most likely result from noise. This is because the function in the nominator of

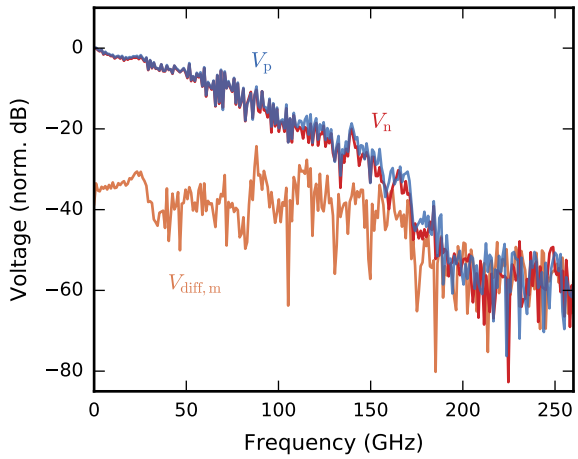

Fig. 4. Power spectrum of the voltage pulses shown in Fig. 3. Plotted are the individual signals V_p and V_n (normalized to 0 dB at dc) as well as the difference signal $V_{diff,m}$.

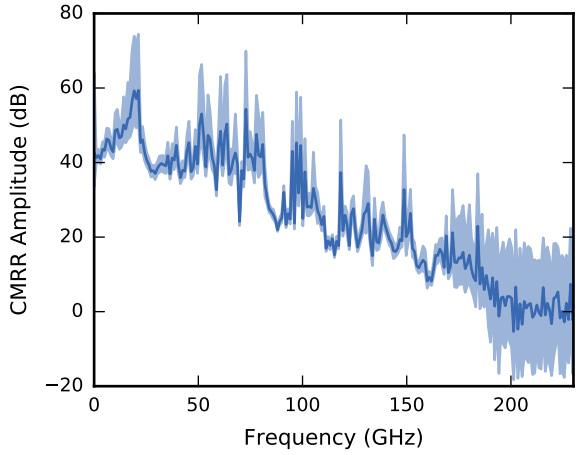

Fig. 5. Optimized CMRR obtained from (4). The light semi-transparent color denotes the 95% confidence intervals.

(4) and (6) approach the noise. It would be interesting to see whether the results will improve by using regularization filters [12], but we defer any further discussion of this issue to a later study.

At the end of this section we comment on the difference between the optimized CMRR and the CMRR obtained from measurements with the same photocurrents. The difference (best estimate including 95% confidence intervals) between the two values is shown in Fig. 6. The optimization mainly improves the CMRR around 20 GHz, where an improvement by 20 dB is obtained. In the same figure we also plotted the difference between the CMRR obtained from optimization of (4) and (6). This plot visualizes that due to the good linearity of the device no significant differences between the two optimization methods exist. As discussed above this is in line with the time-domain results plotted in Fig. 3.

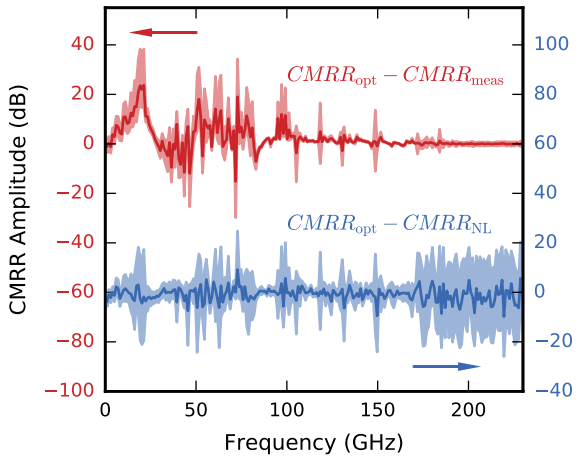

Fig. 6. Red curve: difference between optimized CMMR (4) and the CMRR (1) obtained from the measurements without optimization of $V_p(f)$. Blue curve: difference between the optimized CMRR and the optimized CMMR accounting for a non-linearity of the photodetector under test (6). The light semi-transparent colors denote the 95% confidence intervals.

IV. Use of Commercial Instrumentation

There are only a few primary-standard EOS systems worldwide. However, lower bandwidth commercial systems are available. CMRR (1) is ratiometric and consequently the key instrumentation requirements are linearity, sufficient bandwidth, stability and dynamic range. Moreover, CMRR can be calculated without recourse to the absolute response. In this section we explore the capabilities and limitations achievable using commercial instrumentation that is readily accessible for research and manufacturing.

A. Digital sampling and real-time oscilloscopes

Digital Real-Time Oscilloscopes (DRTO) have superior timebase linearity but a limited dynamic range which can be improved by acquiring a longer epoch and by measuring the waveform and optically balanced residual component. Instruments are available with sufficient bandwidth to satisfy the current needs. DRTOs contain multiple analog-to-digital converters and consequently this creates errors at sub-Nyquist frequencies [13]. The effect of these can be reduced by calibration [14] but these corrections will increase the uncertainties at these frequencies [15]. Alternatively, selecting a comb repetition frequency that fulfills the criteria outlined in [13] will avoid the sub-Nyquist spurs and make the best use of the instrument ADC linearity.

Digital Sampling oscilloscopes (DSO) with bandwidths of 70 GHz and higher meet the key criteria but these instruments also suffer from poor timebase linearity and sample-to-sample timing errors (jitter). Yet, these failings can be corrected algorithmically [16]–[18] and through the use of additional hardware. All the measurements presented have been carried out using DSO instruments.

An erbium-doped fiber-laser, emitting optical pulses, centered at 1560 nm and with a duration of less than 100 fs (FWHM) and repetition rate (*FSR*) at 250 MHz, was used as

the optical source for the measurements, see Fig. 7. A key element of this system was the ease of synchronization of the RF synthesizers to the comb repetition frequency. This was achieved by controlling the laser cavity length and using spectral broadening to allow $(\nu_1 - 2\nu_2)$ interferometry [19] that measures the carrier frequency offset (CEO) using the relationships

$$\nu_1 = nFSR + \nu_0 \tag{8}$$

$$\nu_2 = 2nFSR + \nu_0 \tag{9}$$

where ν is the optical frequency, FSR is the free spectral range of the laser, and n is the harmonic number. Both the locking signals for the repetition rate and CEO are digitally synthesized from the signal of a GSP-disciplined frequency reference with relative accuracy better than 0.5×10^{-13} after 10 ks of GPS locking. Although the measurements could be performed using a free-running laser system this would require dedicated hardware to ensure low-jitter triggering and to provide the timebase correction.

The optical fiber between the laser and photodiodes was kept short to minimize the chromatic dispersion pulse-spreading to less than 1 ps. Free-space optical launch was used to control the relative delay and optical intensity incident on the two photodiodes.

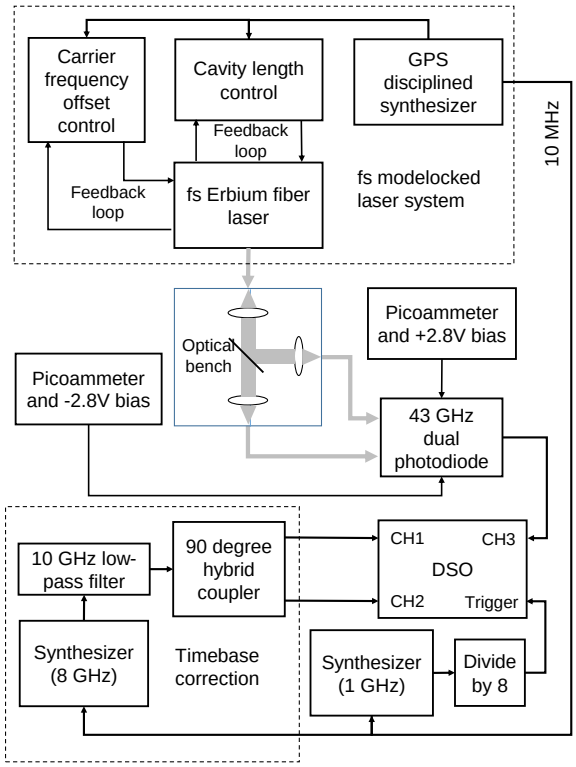

Fig. 7. System layout for the CMRR measurement using the Digital Sampling Oscilloscope (DSO).

The photocurrent for the positive and negative photodiodes were separately monitored and the electrical output waveform was measured directly with the DSO. The timing correction (IQ) was derived from an 8 GHz phase-locked RF signal that was passed through a low-pass filter to remove any residual harmonic components and then applied through a 90-degree hybrid coupler to two channels of the DSO. The IQ signal is therefore harmonically related to the RF comb [20]. The algorithm used [16] does not provide harmonic correction as any residual components have been removed by the low-pass filter. In later measurements a digital divider (÷8) was used to provide a trigger at sub-harmonics of the repetition frequency. This allows the IQ signal to be chosen to avoid the harmonics of the measured RF comb so that intermodulation components caused by residual IQ harmonic contribution do not add coherently to the RF comb [21]. The measurement epoch of 5 ns exceeds the period of the optical waveform.

The measured results, acquired as individual single acquisitions of 16384 points and corrected for timebase nonlinearity display a slight drift over the twenty acquisitions. The initial drift correction was estimated using a variant of the naive autocorrelation approach [22] using one of the waveforms as a reference but this gave a poor CMRR figure of about 20 dB. Applying no drift correction also degrades the result. A simpler correction approach using

$$\tau_j = \frac{\arg\left(\sum_{i=2}^{n} V_{i,j} V_{i-1,j}^{*}\right)}{2\pi FSR} \tag{10}$$

where $V_{i,j}$ is the complex response at the i$^{\text{th}}$ comb harmonic and the j$^{\text{th}}$ measurement gave the best result. As the drift of τ over the measurement run is roughly linear and dominated by the residual noise, a regression fit was used to provide the correction. The drift of the balanced result was dominated by noise and so the average drift of the positive and negative waveforms has been used. Optimization of the the CMRR was done as detailed in Sec. II. The optimized CMRR values calculated using the positive and negative voltage pulses, V_{p} and V_{n}, and the difference and either a positive or a negative voltage pulse, $V_{\text{diff,m}}$ and V_{n}, or ,$V_{\text{diff,m}}$ and V_{p}, are in agreement, see Fig. 8(a). This result confirms the findings obtained from EOS measurements.

The residual uncertainty, due to noise, for each measurement was calculated on the assumption that the underlying measured waveform is time-invariant and that the dominant noise, arising from the sampler, is normally distributed. In this case the resulting best estimate and the 95% confidence interval of the CMRR were obtained from five DSO measurement runs each consisting of twenty waveform acquisitions of v_{n}, v_{p}, and $v_{\text{diff,m}}$, see Fig. 8(b).

B. Vector Network Analyzer

High-performance Vector Network Analyzers (VNA) are likely to be available as a diagnostic instrument within an opto-electronic development or production environment. Although commercial instruments with integral optical modulation are available we have used a 65 GHz (1.85 mm connector) instrument giving approximately -7 dBm (31.5 mV rms), verified with a RF power meter. The system layout of the VNA measurements is shown in Fig. 9. Conversion to an optical modulated signal was achieved using an Integrated Optic Modulator (IOM) with a nominal 20 GHz bandwidth and V_π = 5.8 V and a 1528 nm DFB laser was used as the

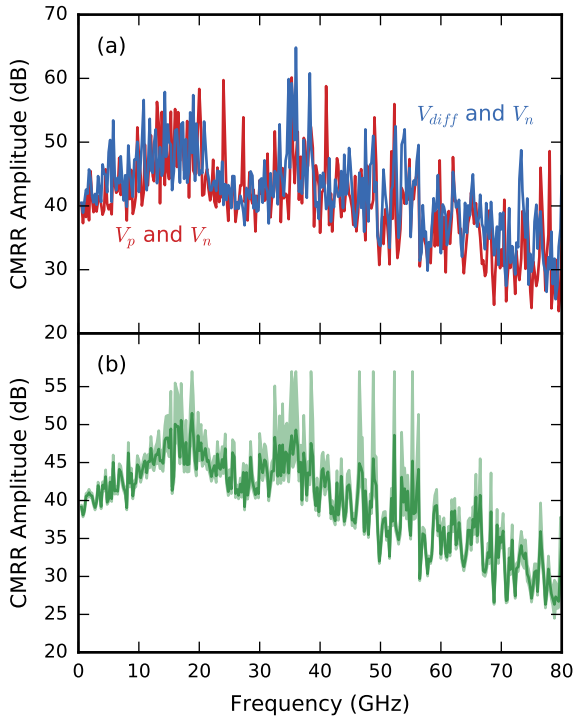

Fig. 8. (a) Optimized CMRR calculated from DSO measurements using the positive and negative voltage responses, V_{p} and V_{n}, and the difference and the negative voltage responses, $V_{\mathrm{diff,m}}$ and V_{n}. (b) Best estimate of the CMRR. The light semi-transparent color denotes the 95% confidence intervals.

optical source. The upper frequency limit was restricted to 40 GHz, corresponding to the maximum operating frequency of the 2.92 mm connector on the IOM.

We performed individual measurements of each diode (V_{n}, V_{p}) and differential measurements ($V_{\mathrm{diff,m}}$) through an optical coupler. Optimization of the the CMRR was again done as detailed in Sec. II. As we wanted to ensure that the measurements form a single, unique minimum the minimization results were evaluated in the neighbourhood of the minimum as a map. Although this approach is very crude it is sufficient to show that the characteristic is well behaved and would be suitable for a more sophisticated optimization.

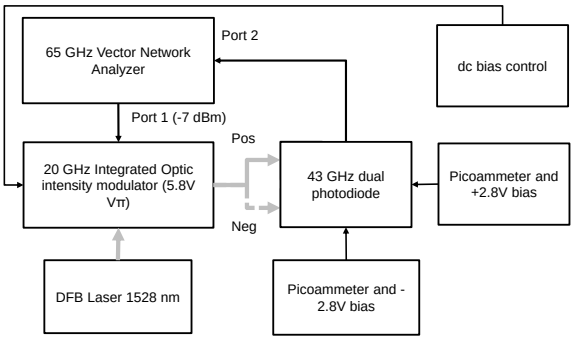

Fig. 9. System layout to measure the dual photodiode frequency response using an Integrated Optic Modulator.

During the measurements the operating current for the photodiode was in the range (0.4-1.0) mA and the bias voltage was ±2.8 V. The acquired results comprise two full waveform sets (V_{p} and V_{n}), two differential sets (V_{p}, V_{n}, and $V_{\mathrm{diff,m}}$), and two noise waveforms. The results obtained with the full waveform and the first difference waveforms are in good agreement but the second differential response with V_{p} and V_{n} gives a lower result at low frequencies, see blue curve in Fig. 10(a). The uncertainty component comprises two terms: the VNA noise contribution, based on a trace without the optical traces and the standard uncertainty of the results. The CMRR results are plotted in dB and so an upper limit uncertainty threshold has been included. The overall CMRR result and uncertainties estimated using all the data are shown in Fig. 10(b).

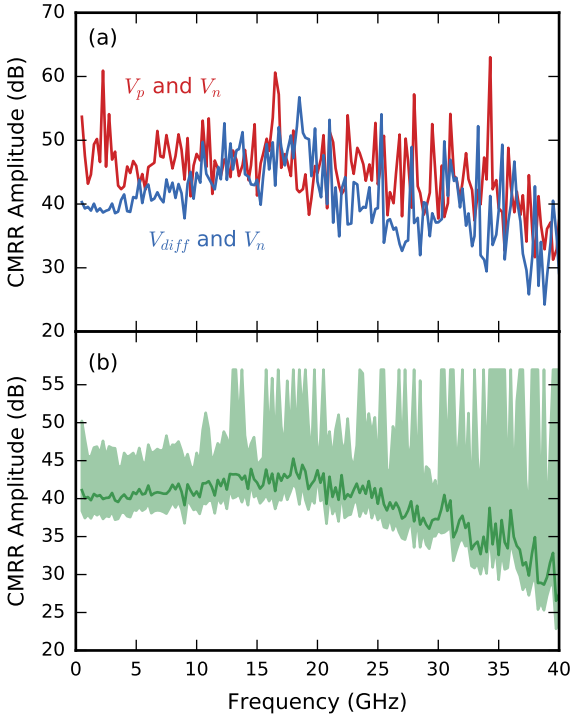

Fig. 10. (a) CMRR calculated from VNA measurements using the positive and negative voltage response, V_{p} and V_{n}, and the difference and the negative voltage responses, $V_{\mathrm{diff,m}}$ and V_{n}. (b) Best estimate of the CMRR. The light semi-transparent color denotes the 95% confidence intervals.

V. Comparison and Conclusions

The optimized results show that the photodiodes are well matched in terms of the RF performance in order to achieve a high level CMRR across the band, greatly exceeding the specified performance of 15 dB. It is important to note that the maximum CMRR does not always occur when the photocurrents are exactly equal. This may influence the best practice for active optical alignment of coherent detectors if the "best" result can be achieved by minimizing the RF power when both devices are illuminated.

The CMRR obtained with the three different techniques is shown in Fig. 11. Measurements with commercial DSO and VNA systems show that these instruments can measure

a CMRR of at least 50 dB (DSO) and 45 dB (VNA, see also discussion below), but the upper frequency limit is significantly less than that available with the EOS, see Fig. 5. The VNA covered the lowest bandwidth due to the 20 GHz optical modulator and the low RF power used (-7 dBm), whereas the DSO was useable beyond its specified upper-frequency (≈70 GHz, 1.85 mm coaxial connector) because the measurement is ratiometric and the RF connectors were not disturbed during the measurement.

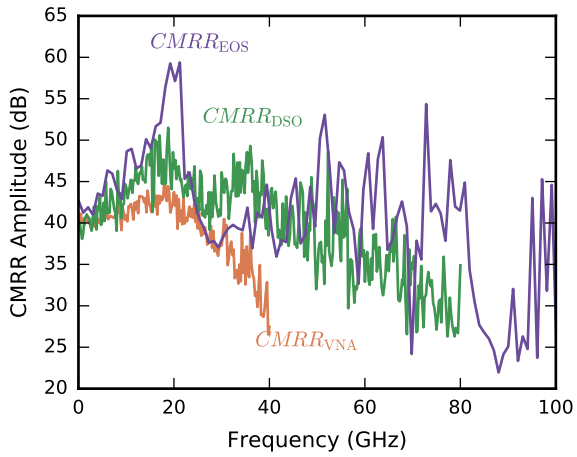

Fig. 11. Comparison of the CMRR obtained with the three different techniques. The coverage intervals have been omitted for clarity.

Comparing the curves of Fig. 11 with each other, we obtain a reasonable agreement. In particular the DSO and EOS results show very similar frequency-dependent features such as an increase of the CMRR up to 20 GHz and a subsequent decrease up to 30 GHz. Yet, we also note that at 20 GHz and 50 GHz and around 60 GHz the differences between DSO and EOS results are larger than 10 dB. Although the 95% coverage intervals are large at these particular frequencies we find that the intervals do not fully overlap across the whole frequency range. We attribute this finding to the fact that the optimized CMRR depends on the frequency range (which is larger for the EOS than for the DSO measurements) and on the frequency spacing (which is smaller for the DSO than for the EOS measurements). A more detailed study of these influences is beyond the scope of this work. The differences between the DSO and EOS results above 70 GHz most likely result from the limited bandwidth of the DSO. Similarly the decrease of the VNA result above 30 GHz is due to the low bandwidth of the optical modulator. We believe that by using a higher bandwidth modulator and a broadband amplifier an improvement of the CMRR measurement of 10 dB is achievable. Ultimately, the limit will be set by residual nonlinearities in the VNA and the amplifier.

The critical dependence of the CMRR value on linear instrument corrections, such as waveform time-alignment and timebase correction suggest that these additional corrections are necessary to achieve a high CMRR result. The photodiode measurements were restricted to about 150 mV peak. The diode can be used at higher pulse levels, with the risk of some nonlinearity from the device under test or from the DSO.

In conclusion, a CMRR system comprising of commercial instrumentation, such as a DSO and optical pulse source or a VNA, DFB and high-bandwidth modulator and can be realized. The results compare well to measurements using EOS techniques based on femtosecond lasers, which will even allow the methods using commercial instrumentation to be optimized.

ACKNOWLEDGMENT

The authors thank Finisar Corporation for the loan of balanced detectors and Andreas Umbach and Andreas Steffan for enlightening discussions. David Humphreys thanks Robert Fergusson, NPL, for the loan of the portable optical table and associated optical equipment to perform the measurements at University of Sussex.

REFERENCES

[1] S. Malyshev and A. Chizh, "State of the art high-speed photodetectors for microwave photonics application," *15th International Conference on Microwaves, Radar and Wireless Communications, 2004. MIKON-2004*, vol. 3, pp. 765–775, 2004.

[2] M. Wada, T. Yakihara, and A. Miura, "High-speed photodetectors for full-wavelength-band WDM transmission systems at 40Gb/s and beyond," *Proc. SPIE*, vol. 5624, pp. 391–398, 2005.

[3] L. K. Anderson and B. J. McMurtry, "High-speed photodetectors," *Proc. of the IEEE*, vol. 54, no. 10, pp. 1335–1349, 1966.

[4] T. Morimune, H. Kajii, and Y. Ohmori, "Frequency response properties of organic photo-detectors as opto-electrical conversion devices," *J. Display Technol.*, vol. 2, no. 2, pp. 170–174, Jun 2006.

[5] Y. Painchaud, M. Poulin, M. Morin, and M. Têtu, "Performance of balanced detection in a coherent receiver," *Opt. Express*, vol. 17, no. 5, pp. 3659–3672, Mar 2009.

[6] X. Jin, J. Su, Y. Zheng, C. Chen, W. Wang, and K. Peng, "Balanced homodyne detection with high common mode rejection ratio based on parameter compensation of two arbitrary photodiodes," *Opt. Express*, vol. 23, p. 23859, Sep. 2015.

[7] A. Beling, H. G. Bach, D. Schmidt, G. G. Mekonnen, M. Rohde, L. Molle, H. Ehlers, and A. Umbach, "High-speed balanced photodetector module with 20db broadband common-mode rejection ratio," in *Optical Fiber Communication Conference*. Optical Society of America, 2003, p. WF4.

[8] Webpage of Finisar Corporation. [Online]. Available: www.finisar.com

[9] D. O. Otuya, K. Kasai, T. Hirooka, and M. Nakazawa, "Coherent Nyquist orthogonal TDM transmission with a spectral efficiency of 10.6 Bit/s/Hz," *Journal of Lightwave Technology*, vol. 34, no. 2, pp. 768–775, Jan 2016.

[10] D. Williams, A. Lewandowski, T. Clement, J. Wang, P. Hale, J. Morgan, D. Keenan, and A. Dienstfrey, "Covariance-based uncertainty analysis of the NIST electrooptic sampling system," *IEEE Trans. Microw. Theory Tech.*, vol. 54, pp. 481–491, 2006.

[11] P. Struszewski and M. Bieler, "Characterization of high-speed photodetectors using a laser-based vector network analyzer," in *Conference on Precision Electromagnetic Measurements (CPEM)*, Ottawa, Canada, 10-15 July 2016.

[12] M. Bieler, H. Füser, and K. Pierz, "Time-Domain Optoelectronic Vector Network Analysis on Coplanar Waveguides," *IEEE Trans. Microw. Theory Tech.*, vol. 63, no. 11, pp. 3775–3784, Nov. 2015.

[13] D. A. Humphreys, M. Hudlicka, and I. Fatadin, "Calibration of wideband digital real-time oscilloscopes," in *Precision Electromagnetic Measurements (CPEM 2014), 2014 Conference on*, Aug 2014, pp. 698–699.

[14] C. Cho, J. G. Lee, P. D. Hale, J. A. Jargon, P. Jeavons, J. Schlager, and A. Dienstfrey, "Calibration of channel mismatch in time-interleaved real-time digital oscilloscopes," in *Microwave Measurement Conference (ARFTG), 2015 85th*, May 2015, pp. 1–5.

[15] D. A. Humphreys, P. M. Harris, M. Rodríguez-Higuero, F. A. Mubarak, D. Zhao, and K. Ojasalo, "Principal component compression method for covariance matrices used for uncertainty propagation," *IEEE Trans. Instrum. Meas.*, vol. 64, no. 2, pp. 356–365, Feb 2015.

[16] D. A. Humphreys and F. Bernard, “Compensation of sampling oscilloscope trigger jitter by an in-phase and quadrature referencing technique,” *ARMMS Conf., Abbingdon, UK*, April,18-19 2005.
[17] P. D. Hale, C. M. Wang, D. F. Williams, K. A. Remley, and J. D. Wepman, “Compensation of random and systematic timing errors in sampling oscilloscopes,” *IEEE Trans. Instrum. Meas.*, vol. 55, no. 6, pp. 2146–2154, Dec 2006.
[18] G. Vandersteen, Y. Rolain, and J. Schoukens, “An identification technique for data acquisition characterization in the presence of nonlinear distortions and time base distortions,” *IEEE Trans. Instrum. Meas.*, vol. 50, no. 5, pp. 1355–1363, Oct 2001.
[19] T. Udem, R. Holzwarth, and T. W. Hänsch, “Optical frequency metrology,” *Nature*, vol. 416, pp. 233–237, March,14 2002.
[20] H. C. Reader, D. F. Williams, P. D. Hale, and T. S. Clement, “Comb-generator characterization,” *IEEE Trans. Microw. Theory Tech.*, vol. 56, no. 2, pp. 515–521, Feb 2008.
[21] D. A. Humphreys, A. Raffo, G. Bosi, G. Vannini, D. Schreurs, K. N. Gebremicael, and K. Morris, “Maximizing the benefit of existing equipment for nonlinear and communication measurements,” in *2016 87th ARFTG Microwave Measurement Conference (ARFTG)*, May 2016, pp. 1–4.
[22] K. J. Coakley and P. Hale, “Alignment of noisy signals,” *IEEE Trans. Instrum. Meas.*, vol. 50, no. 1, pp. 141–149, Feb 2001.

Paul Struszewski received the master degree in physics from the University of Rostock, Germany, in 2014. Since 2015 he has been with the Physikalisch-Technische Bundesantstalt in Braunschweig. His research in the Working Group "Femtosecond Measurement Techniques" focuses on high-precision GHz and THz metrology and the characterization of high-frequency electric devices.

Mark Bieler received the diploma and Ph.D. in electrical engineering from the Technical University of Braunschweig, Germany, in 1999 and 2003, respectively. He was a Post-Doctoral Fellow with the University of Toronto from 2003 to 2004. Since 2004, he has been with the Physikalisch-Technische Bundesanstalt, Braunschweig, where he is currently the Head of the Femtosecond Measurement Techniques Working Group. He has authored over 100 journal and conference papers. His current research interests include the characterization of high-speed electronic devices, highfrequency electric field measurements, and the investigation of ultrafast photocurrents and carrier kinetics in semiconductors. Dr. Bieler was a recipient of the 2005 German AHMT Messtechnikpreis and the Outstanding Paper 2015 Award from the journal Measurement Science and Technology.

David Humphreys (M’89-SM’90) was born in Epsom, UK in 1956. He received a BSc in electronic engineering from Southampton University, UK in 1978 and a PhD in electronic engineering from London University, UK in 1990. His thesis concerned the accurate measurement of high-speed optoelectronic devices at telecommunication wavelengths. He joined the National Physical Laboratory, Teddington, UK in 1978 and was the coordinator for the EMRP IND51 "Metrology for RF and Optical Communications" joint research project from June 2013 until June 2016. He is Vice-Chair of the P1765 IEEE pre-standards group on "The uncertainties in Error-Vector-Measurement (EVM)". His recent metrology interests include, full-waveform characterization of the primary-standard electro-optic sampling system, RF waveforms for wireless communications, EVM, 5G, nonlinear RF measurements and correlated waveform uncertainties. Dr Humphreys is a Chartered Engineer and a Corporate Member of the IET (UK) and a Research Fellow at the University of Bristol, UK. He was awarded the IEE Ambrose Fleming Premium in 1987 and has published over 90 journal and conference papers.

Hualong Bao was born in Taizhou, Zhejiang Province, China, in 1984. He received his M.Sc degree in Optical Engineering from China Jiliang University, Hangzhou, China, in 2011 and the PhD degree in Optical Engineering from Technical University of Denmark, Lyngby, Denmark, in 2015. He joined the Emergent Photonics Labs in Aug. 2015 as postdoctoral research fellow of the University of Sussex, Brighton, United Kingdom. He is the author of 7 publications on international scientific journals, 8 communications to international conferences and 1 patent. His research interests include fiber optics, terahertz technology, nonlinear integrated Photonics and optical frequency comb.

Marco Peccianti was born in Genoa, Italy in 1973. He received his MSc degree in electronic engineering (Laurea, Magna Cum Laude) in 2000 and the PhD degree in 2004 from the University Roma Tre, Rome, Italy. From 2012, he is part of the of the Global Young Academy. From 2013 he is a faculty of the Dept. of Physics of the University of Sussex where he is now Reader in Physics and director of the Emergent Photonics Labs. He is author of about 95 publications in the most reputed international journals, 200 communications to international conferences and 3 book chapters, with an overall H-index of 33 and about 4200 citations. He is a reviewer for several journal organizations and associate editor of the journal Scientific Reports (NPG). His current research interests includes, the experimental investigation of devices for the enhancement and the manipulation of THz waves and the investigation of nonlinear optical effects in nanostructured integrated optics, from signal processing to ultrafast clocks. He is the inventor of three patents on ultrafast optical pulsed technologies. Marco Peccianti was the recipient of several prizes and personal fellowships, including the Otto Lehmann Award (Karlsruhe, Germany) in the 2005, of a Marie Curie Fellowship in 2008 and of the Marie Curie Career Integration Grant in the 2014.

Alessia Pasquazi was born in Rome, Italy in 1980. She received her MSc degree in electronic engineering (Laurea, Magna Cum Laude) in 2005 and the PhD degree in 2009 from the University Roma Tre, Rome, Italy. She started her research career at University Roma Tre (Italy) and worked at the INRS-EMT, (QC, Canada) as post-doctoral fellow from 2008 to 2013. She is a Senior Lecturer at the University of Sussex (UK), where she moved following the award of the European Marie Curie Incoming Fellowship (EU-FP7). She is the author of 32 publications in international scientific journals of more than 90 publications in international conferences and of two book chapters, with an H-index of 16. She is associate Editor of the journal Scientific Reports (NPG) and regularly serves as a committee member in several panels of IEEE, OSA and SPIE conferences. She is a panel member of the Marie Curie evaluation committee (Horizon 2020 program). Her research interests include the nonlinear dynamics of waves and solitons propagation, mode-locking modelling in dissipative systems, dissipative four wave mixing lasers, integrated optical devices for ultrafast processing, and optical frequency combs. She is inventor of two patents on ultrahigh repetition rate lasers.